Characterization of Foreshock Plasma Populations at Mercury

^r ustin N. Glass¹, Patrick J. Tracy¹, Jim M. Raines¹, Xianzhe Jia¹, Norberto Romanelli^{2,3}, Gina A. DiBraccio³

¹Department of Climate and Space Sciences and Engineering, University of Michigan, Ann Arbor, MI, USA. ²Department of Astronomy, University of Maryland, College Park, MD, USA. ³NASA Goddard Space Flight Center, Greenbelt, MD, USA.

Corresponding author: Austin N. Glass (anglass@umich.edu)

Key Points:

- Mercury's foreshock contains diffuse and field-aligned beam (FAB) populations with similar characteristics to the same populations at Earth
- Diffuse and FAB populations in Mercury's foreshock are organized according to shock geometry in a manner very similar to Earth
- Diffuse and FAB populations are associated with simultaneous wave activity in the magnetic field

Abstract

Observations of foreshock plasma populations at Mercury are presented utilizing measurements from the Fast Imaging Plasma Spectrometer (FIPS) aboard the Mercury Surface, Space Environment, Geochemistry, and Ranging (MESSENGER) spacecraft. The magnetosphere and foreshock system at Mercury exists in a unique parameter space, due to the planet's relatively weak magnetic dipole and the proximity of its orbit to the Sun. Previous investigations have therefore questioned whether there is sufficient free energy at Mercury to generate foreshock populations, due to the small spatial scale of its bow shock. The observations presented in this work show that field-aligned beam and diffuse populations similar to those seen in the terrestrial foreshock are able to form upstream of the Hermean bow shock. The observed populations are organized by the bow shock geometry, and are associated with magnetic wave activity previously detected in Mercury's foreshock with corollaries to the terrestrial foreshock.

Plain Language Summary

Upstream of a magnetized planet sitting in supersonic flow, a region is formed called the "bow shock", which acts to slow down the flow before it impacts the obstacle. Because of the dynamic magnetic field environment, the bow shock can also act to speed up a fraction of the population, directing the ions back upstream. These processes have been described at Earth; here, we document observations of nearly 40 foreshock plasma populations observed at Mercury, and compare them to the populations at Earth. Despite Mercury's proximity to the Sun relative to Earth, we find that the two foreshock environments are very similar, with a few key differences worthy of future study.

1 Introduction

The terrestrial bow shock has been the primary focus for studies of the acceleration of ions at collisionless shock for more than half a century (Burgess et al., 2012; Parks et al., 2017). The region directly upstream of the bow shock hosts a variety of different plasma populations whose creation stems, directly and indirectly, from the interaction of solar wind ions with the shock. This "foreshock" region, which is magnetically connected to the bow shock, exhibits a large variety of waves and energized particles. The nature of the magnetic connections between the interplanetary magnetic field (IMF) and bow shock controls the spatial distribution of these populations.

In regions where the angle between the IMF and the bow shock normal (θ_{bn}) is greater than 45 degrees (referred to as quasi-perpendicular), collimated ion beams with energies of a few keV are seen to propagate in the sunward direction along the IMF direction (Paschmann et al., 1980). These ion populations are typically referred to as Field Aligned Beams (FABs), for this reason. Apart from their narrow pitch angle extent, FABs are distinguished by their temperature anisotropies (Paschmann et al., 1981), depletion of He²⁺ relative to the solar wind (Ipavich et al., 1988), and large variation in velocity and density with varying θ_{bn} (Oka et al., 2005). The most widely accepted acceleration mechanism for FABs is the Shock Drift Acceleration (SDA) mechanism (Burgess, 1987). In this mechanism, FAB ions have multiple encounters with the shock as they drift along the convective electric field (in the frame of the shock). This mechanism is broadly consistent with earlier work in which conservation of the magnetic moment, μ , during reflection at the shock in the deHoffman-Teller frame was used to explain FAB acceleration (Sonnerup, 1969). The low relative abundance of alpha particles in FABs was also confirmed in hybrid simulation (Burgess, 1989). A model for FAB acceleration involving the leakage of heated downstream plasma was proposed by Edmiston et al. (1982) and Tanaka et al. (1983), but unlike SDA has not been sufficient to explain observations of FABs at Earth (Möbius et al., 2001; Kucharek et al., 2004; Oka et al., 2005).

The second foreshock population documented by the earliest studies of Earth's foreshock is the diffuse population, which at Earth is generally limited to the quasi-parallel foreshock (where $\theta_{bn} < 45^{\circ}$). Diffuse ions are observed at Earth as a wide, shell-like distribution in velocity space that can extend well above 100 keV in energy (Paschmann et al., 1981). This population type is further characterized by having a relative abundance of He²⁺ comparable to the upstream solar wind (Ipavich et al., 1984), in contrast to the depletion seen in FABs. The coexistence of low frequency waves with observations of diffuse populations was first demonstrated by Paschmann et al. (1979), and further analyzed by Hoppe et al. (1981). Another key observation is that the distributions of diffuse ion populations are well fit by an exponential function in energy (Ipavich et al., 1979). Specifically, the spectra of ions with different charge states (H⁺, He²⁺, and C, N, O ions) are similar when organized by energy per charge.

Early studies of Earth's foreshock, in particular the influential two-part work by Bonifazi & Moreno (1981a, 1981b), distinguished between these two population types based on the ratio between the backstreaming ion bulk velocity and the root-mean-square thermal speed in the spacecraft reference frame. However, it was observed even at that time that the distribution of the frequency of foreshock events according to this ratio was not bimodal, but rather nearly monotonically decreasing. As a result, those authors followed earlier work by strictly separating the diffuse populations from the field-aligned beams and characterizing any population which could not be clearly distinguished as diffuse or as a FAB as "intermediate" to those two population types. The intermediate population type is a bulk-flowing beam in the field-aligned direction like an FAB but has a significantly wider distribution in pitch angle space, resulting in a kidney-bean shape of the velocity distribution function, in a plane which includes the bulk velocity and magnetic field vectors (Kempf et al., 2015). Notably, the distribution of the intermediate population has only backstreaming ions (i.e., with pitch angles within 90° of the parallel or antiparallel direction, depending on which is the sunward direction). This allows clean separation of populations of this type from diffuse ion populations, even while the meaning of the "nearly-collimated" FAB relative to the wider intermediate type remains more qualitative.

Owing to the difficulty in cleanly distinguishing these populations based on scalar moments of their distributions, the earliest theory unifying their observation described FABs as the source population, and the cause, of the intermediate and diffuse populations (Gary et al., 1981; Winske & Leroy, 1984). This theory was consistent with the information available at the time: that the SDA mechanism works effectively to generate FABs, and that the flow of FABs against the solar wind generates waves at a frequency appropriate to influence the foreshock populations. In contrast to this direct wave source mechanism however, later studies of Earth's foreshock with more advanced instrumentation demonstrated that an entirely different acceleration process takes place at the quasi-parallel shock (Gosling et al., 1982, 1989). Because of these findings of an effective first-order Fermi acceleration process unrelated to FAB scattering, the proposed model of diffuse ions as sourced from FABs solely through waveparticle interactions is insufficient to explain the occurrence of diffuse foreshock; a unifying theory for these two energization mechanisms has not yet been widely agreed upon. A comprehensive review of foreshock observations at Earth is presented in Burgess et al. (2012). Beyond spacecraft observations at Earth, using a global kinetic model Omidi et al. (2005) and Blanco-Cano et al. (2006) showed that magnetospheres with a magnetopause standoff distance greater than only a single ion skin depth can cause the generation of an Earth-like quasiperpendicular foreshock environment. Additionally, observations from Venus and Mars have demonstrated the presence of FABs in the foreshocks of both planets (Yamauchi et al., 2011), and the presence of ULF waves at Venus, which are likely caused by these backstreaming ions (Shan et al., 2016, 2018). A comprehensive review of foreshock observations and modeling throughout the solar system is presented in (Zhang et al., 2022).

Magnetic field waves upstream of Mercury's bow shock were observed as early as 1974 using data from one of the Mariner 10 flybys (Fairfield & Behannon, 1976). In this initial work, two wave modes were identified: a whistler mode wave with relatively high-frequency and low-amplitude, present over a range of upstream conditions with a sharp cutoff at between 2 and 4 Hz; and a low-frequency, high-amplitude wave mode with frequency between 0.1 and 0.2 Hz in the region upstream of the quasi-parallel shock. The lowest-frequency wave was seen to have similar characteristics to the so-called "30-second" waves (owing to the observed wave period in the spacecraft reference frame), which are associated with back-propagating diffuse plasma populations at Earth. Further study using measurements from MESSENGER during a single Hermean foreshock passage by Le et al. (2013) found the lowest frequency waves had an observed frequency of 0.3 Hz. This work also identified a third wave mode of frequency approximately 0.8 Hz, which is sporadically present along with the slightly higher-frequency whistler mode waves.

At Earth, waves of the second wave mode (with periods of about 30 seconds) have been previously associated with the fast magnetosonic waves generated by backstreaming protons (FABs) in the foreshock (Hoppe et al., 1981). A recent analysis of waves in the 0.05 - 0.41 Hz range has shown the lowest frequency wave mode at the Hermean foreshock is also characterized by a lower normalized wave amplitude and occurrence rate relative to the terrestrial foreshock (Romanelli et al., 2020). That work also estimated that the bulk velocity of resonant backstreaming proton populations parallel to the magnetic field (in the solar wind reference frame) ranges between 0.95 and 2.6 times the solar wind speed. Moreover, Romanelli & DiBraccio (2021) found that the ultra-low frequency wave occurrence rate increases with Mercury's heliocentric distance and that the conditions for backstreaming protons are potentially present throughout Mercury's orbit, its high eccentricity notwithstanding. In addition, Jarvinen et al. (2020) uses a global 3D hybrid model to investigate the main properties of the Hermean foreshock under perihelion conditions. The authors report favorable conditions for the generation of back streaming ion populations with bulk velocities much lower than the solar wind bulk velocity, and the presence of low frequency waves with similar characteristics to the ones reported in Romanelli & DiBraccio (2021).

The motivation to study foreshock populations at Mercury stems from the fact that its foreshock environment exists in such a different parameter space to Earth's. This parameter space is roughly outlined in Slavin & Holzer (1981), where the values critical to planetary bow shocks are estimated. Key comparisons are that the sonic and Aflvénic Mach numbers are lower by a about a factor of 2, and the Parker spiral configuration is significantly more radial as compared to the situation at Earth. Furthermore, Ogilvie et al. (1977) and Winslow et al. (2013) establish the scaling of magnetosphere size between Earth and Mercury, with Mercury's bow shock scale about an order of magnitude smaller than Earth's.

This new parameter space raises the question of whether a foreshock at Mercury is at all similar to that seen at Earth. Preliminary analysis of MESSENGER magnetometer data has suggested that waves seen almost continuously in Earth's foreshock and associated with diffuse populations at Earth ("30-second" waves) are only sporadically seen at Mercury (Le et al., 2013). It has been suggested that the absence of these waves implies that the small spatial scale of Mercury's bow shock limits the formation of a diffuse population at Mercury. Likewise with the small spatial size of Mercury's bow shock there is a question of whether the planar shock drift acceleration mechanism can act or if bow shock curvature effects are strong enough to preclude it. While there have been numerous observations of foreshock events upstream of Earth's bow shock, the current analysis of Mercury's foreshock has been lacking in substantial plasma measurements. At stake is the question of how the smaller scale size, and different ambient solar wind conditions, impact the observed Hermean foreshock environment.

Despite similarities between the plasma-associated waves of Earth's foreshock and the waves measured at Mercury, no previous work has yet attempted to identify foreshock plasma populations at Mercury, nor to correlate such plasma observations with wave measurements. The concurrent magnetic field and plasma measurements made by instruments aboard MESSENGER has allowed us to perform this analysis. In this article's description of our work, we first present and characterize two easily-identifiable examples of plasma populations in Mercury's foreshock. We then discuss statistics derived from a set of 39 high-quality observations of additional occurrences of these two population types in Mercury's foreshock, across the first 3000 orbits of the MESSENGER spacecraft at Mercury. A correlation between our plasma observations and observations of simultaneous magnetic field wave activity previously observed at Mercury follows, and we conclude with a discussion of potential for future work.

2 Identification of Foreshock Populations

The identification of foreshock plasma populations at Mercury is made possible by the measurements of the Fast Imaging Plasma Spectrometer (FIPS). FIPS measured the mass per charge (m/q) and energy per charge (E/q) of incident ions with time of flight (TOF) mass spectrometry. The electrostatic analyzer of FIPS had an instantaneous field of view of about 1.4π sr and can record the arrival direction of incident ions with an angular resolution of about 15 degrees. Due to FIPS position on MESSENGER, its FOV was partially obstructed by the sunshade and other parts of the spacecraft. Accounting for these obstructions, the FOV of FIPS was approximately 1.15π sr (Gershman et al., 2013).

The TOF measurements of FIPS allow for separation of m/q between 1 and 40 amu/e. For the data presented here, FIPS was operating with 60 logarithmically spaced E/q steps with an integration time of 50 ms at each step and a total scanning time of about 10 seconds. Depending on the time range in our period, the steps were either spaced from 100 eV/e to 13.3 keV/e or 46eV/e to 13.3 keV/e, as the low E/q bound of the instrument was lowered in August of 2012. For more details on FIPS operation and its capabilities see Andrews et al. (2007). The analysis presented in this work will primarily focus on proton data measured by FIPS. Although FIPS has the ability to observe heavy ions, the small number that were observed in the foreshock region at

Mercury did not permit a detailed analysis. Unless otherwise mentioned, all following analysis pertains entirely to proton measurements.

The identification and characterization of wave activity at Mercury is performed using magnetic field measurements of the MAG instrument, with a cadence of 20 samples per second and a resolution of 0.047 nT (Anderson et al., 2007).

2.1 Field-Aligned Beams

Our identification of FABs makes extensive use of the incident ion direction abilities of FIPS. We begin with an example of a FAB population that occurred on 2012-09-19 at about 14:20. The multi-paneled time series of relevant FIPS and MAG measurements for this period is shown in Figure 1. An observation of a FAB population occurred between 14:20 and just after 15:00, in the region just upstream of a quasi-perpendicular bow shock. The general quasi-perpendicular nature of the shock is revealed by the sharp increase in the magnitude of B as the bow shock is crossed and MESSENGER enters the magnetosheath at about 15:03.

In the E/q spectrogram, two populations are clearly seen during the FAB event period, one at low E/q and one at higher E/q values. Noting that the lower E/q population is consistent with solar wind energies allows us to identify the higher E/q population as an energized population in the foreshock, but without the directional capabilities of FIPS it would be very difficult to discern the population type.

In Figure 2, the angular distribution of the plasma measured by FIPS with E/q between 0.3 and 1 keV are plotted. The center of this Mollweide projection corresponds to plasma traveling in an antisunward direction; plasma traveling in duskward direction would fall on the "Dusk" label, and so on. Solar wind observed by FIPS should be aberrated due to Mercury's orbital motion about the Sun, and indeed we see that the portion of the solar wind visible by FIPS here was aberrated in the duskward direction, enabling it to pass around the heat shield of the MESSENGER spacecraft (Gershman et al., 2012). The important point in Figure 2 is simply that the observed plasma has an antisunward velocity direction consistent with the solar wind.

In Figure 3, we show two energy resolved pitch angle distributions. In the left panel, we show the solar wind beam in the frame of the spacecraft, portraying its typical angular width and energy range. In the right panel, now in the frame of the solar wind, it is clear to see that the higher energy population present during the event period in Figure 1 was closely aligned with the anti-parallel magnetic field direction, given that its pitch angle distribution peaks approaching 180 degrees, and doesn't extend much beyond 90 degrees. This observation of a beam of plasma aligned with the magnetic field in the solar wind frame matches the characteristics for FABs observed at Earth.

The last step in the identification of this FAB is to quantify the moments of the observed distribution. As this FAB was a supersonic distribution, the techniques developed in Gershman et al. (2012) for solar wind observations by FIPS are directly applicable to the recovery of the moments. The only difference between the analysis in that work and the present analysis is that, to our benefit, the core of the FAB distribution lies within the FOV of the FIPS instrument (whereas the core of the supersonic solar wind distribution studied in that work was obscured by the MESSENGER spacecraft's heat shield). Because the core of the distribution falls within the FOV, an accurate density for the FAB can be recovered.

The measured count distribution and phase space distribution for the FAB event in the spacecraft reference frame are shown in Figure 4. The top panel shows the count distribution for the solar wind which is shaded in green while that for the FAB is shaded in blue. Two peaks, clearly separated in velocity space, are observed. In the bottom panel, this count distribution is then converted to phase space density (Gershman et al., 2013), where it is more obvious that the FAB population had a much lower density than the typical ambient solar wind at Mercury (Slavin & Holzer, 1981). For reference, the phase space density corresponding to a single observed count at each velocity bin of FIPS is shown with the dashed line. For the solar wind population (because the core of the distribution is obscured) only the bulk velocity and thermal velocity can be reliably recovered (Gershman et al., 2012); those recovered values are shown in the figure title, according to their definitions in that work. The recovered density, bulk velocity, and thermal velocity for the FAB event are also shown in the title, following the same definitions.

The recovery scheme shown here was also implemented for the 14 other best FAB populations identified so far with FIPS measurements. A summary of the recovered density, temperature and bulk velocity for these FAB populations is discussed in detail after the presentation of the diffuse event in the next section.

2.2 Diffuse Events

The accurate identification of diffuse foreshock populations also requires the full directional capabilities of the FIPS instrument. To illustrate the process, which has a large degree of overlap with the FAB identification process, we show the details of the identification of the diffuse event which occurred on December 5th, 2012 during a period ranging from 06:30 to 07:40 UTC. In the top panel of Figure 5, a time series of the energy spectrogram for this full period is shown. The spacecraft begins upstream of the foreshock in a region without significant plasma present; briefly observes a plasma population from about 06:33:40 to 06:37:40; and then continues to observe a similar-looking population from 06:40 until it crosses the shock at around 07:22. After this point, the spacecraft observes the magnetosheath, and then enters the closed field region of the dayside magnetosphere at just before 07:35. The remaining panels of the figure show a zoomed-in view of the foreshock population region, in the style of Figure 1.

At the outset of investigation of the foreshock population present here, we take note of the striking temporal correlation between the plasma observations and observations of noncompressional magnetic waves (with significant amplitudes occurring mostly in the components perpendicular to the dominant MSO x direction). The Fourier transform of the magnetic field in this region is consistent with the presence of .3 Hz waves – those identified before at Mercury as being analogous to 30-second waves at Earth, the mode observed concurrently with diffuse ions there. However, just as for the FAB, direct confirmation that this population has the same plasma character as a diffuse population relies on the angular distribution measurements of the FIPS instrument.

In Figure 6 we show the energy resolved pitch angle distribution for the time period from Figure 5, as in Figure 3. As no solar wind is observable by FIPS during the event period, the full E/q range is shown, and it is clear that the observed distribution is a very broad and very hot population, as evident in its high width in both the radial and angular direction, respectively. Characteristic of a diffuse population, it is much more broadly distributed in pitch angle than the

FAB, including a significant component streaming toward the shock, in the region of velocity space observable by FIPS in the solar wind frame.

The last step in identifying diffuse populations is examination of the count and phase space distributions. Figure 7 shows the distribution of the diffuse population (blue) within the entire FIPS distribution function summed over pitch angle, in the spacecraft reference frame. The top and bottom panels are presented in the same format as Figure 4, although there are clear differences between the diffuse and FAB populations. Most prominently, unlike the FAB the diffuse population does not show up as a distinct peak in the phase space distribution, instead manifesting as a highly thermal tail to what is likely a very small streaming velocity. The recovery of the bulk plasma parameters for the diffuse populations can be achieved by using assumptions similar to those in Gershman et al. (2013). In that work they assumed an isotropic Maxwellian distribution for observations of magnetosheath plasma, with an assumption of low Mach number, to evaluate the bulk parameters of the observed plasma. We will also assume isotropy in the spacecraft frame, in which the diffuse populations we observe are even more evenly distributed. In the recovery method of Gershman et al. (2013), they assume the Maxwellian plasma distribution isn't well observed below some lower velocity bound. That assumption can be complicated for the case of some diffuse population observations, especially those in which the solar wind is simultaneously observed. There is some evidence at Earth (Paschmann et al., 1981) that there is not any substantial amount of the population at these low velocities, but the lack of observations could also be dependent on the distance of the observation from the bow shock (Kis et al., 2004). Lower velocity diffuse ions would have less ability to diffuse upstream, and therefore may not be observed at large distances from the bow shock.

Limited as we are by the measurements available, in our calculations of the plasma moments for diffuse populations we ignore the portion of the diffuse population that is below the lower E/q cut (see Figure 7), implicitly assuming it has a negligible phase space density. Based on the small fraction of the isotropic diffuse event visible in the range of solar wind energies, this assumption likely only results in a small underestimate of the density and small overestimate the thermal velocity of our observed diffuse distribution, which is also true in the recovered results for the remainder of events in the survey. By assuming a low Mach number (or a thermal velocity much greater than the bulk velocity), we are essentially assuming that the bulk velocities of the diffuse populations are zero in the spacecraft frame, and therefore aren't recoverable with this scheme. The recovered plasma parameters for the solar wind and diffuse populations in our example diffuse event are shown in the plot title of Figure 7.

3 Survey Findings

As noted earlier, the moment recovery techniques applied in the previous section have been applied to a larger set of the 15 best-quality FABs; and we have additionally applied the same to 24 of the best-quality diffuse events observed during MESSENGER's first 3000 orbits of Mercury.

For FABs, the extracted density values have a mean value of about 1.2 per cm³; the least dense event has a density of just over 0.2 per cm³, while the densest has a density of just over 3.1 per cm³. At Earth, FABs are found to have densities between 0.3% and 15% of the density of the solar wind (Burgess et al., 2012). Although the MESSENGER mission was not able to make direct measurements of the solar wind density, the density values we find for FABs at Mercury range between 0.32% and 9.8% of the density of the most and least dense solar wind predicted at

Mercury, respectively (Slavin & Holzer, 1981). The mean temperature of the measured FABs is 1.4 MK, with values ranging from 0.6 MK to 2.9 MK; and the mean velocity of the measured FABs is 570 km/s, ranging from 456 km/s to 870 km/s.

For diffuse events, the extracted density values are similar to the FABs, with a mean value of 1.6 per cm³; the least dense event has a density of just over 0.4 per cm³, while the densest has a density of 5 per cm³. Although the mean density of diffuse events in our survey is slightly higher than the mean density of FABs, this difference is likely on the same scale as the margin of error for our measurements and approach. At Earth, typical diffuse populations are found to have densities of about 2% of the density of the solar wind (Burgess et al., 2012); the density of diffuse populations at Mercury in this survey falls between 2.2% and 5% of the most and least dense solar wind predicted at Mercury, respectively – only modestly higher than the anticipated value based on Earth observations. Unlike density, the temperature distribution of diffuse populations is quite different to that of FABs; the average temperature for the diffuse events in this survey is 51 MK, ranging from 26 to 97 MK. These findings are consistent with the observations at Earth, and now at Mercury, of diffuse events as a high-energy tail on the solar wind distribution at velocities higher than the solar wind speed (which equates to about 20 MK).

3.1 Characterization of Population Origins

With our identification of a survey sample of FAB populations and diffuse populations in the foreshock at Mercury we next aim to highlight the spatial distribution of the events. This is the first time these events have been observed at Mercury and therefore any differences in the general appearance of the foreshock region between Mercury and Earth are especially valuable.

At Earth, the foreshock is typically drawn with a clearly organized boundary between regions where the energization mechanisms for FABs and diffuse populations are most effective. Under a typical IMF orientation, diffuse populations tend to appear on the dawn side of the bow shock and FABs on the dusk side. There are also observations at the boundary of these regions where both populations were observed at the same time (Kis et al., 2007). As this organization is a prominent feature in the terrestrial foreshock, we investigate the organization of events in Mercury's foreshock, according both to location of observation and inferred origination point at the shock surface.

Based on average spacecraft location during observation of each of the 39 events in our study, we find that both FABs and diffuse populations occur across almost the entirety of the foreshock region sampled by the MESSENGER spacecraft. We find FABs between 6 and 17 local time, and between -80 and 10 degrees magnetic latitude (because of MESSENGER's polar orbit with periapsis in the northern hemisphere, it did not sample the foreshock at high latitude in the northern hemisphere); and we find diffuse populations between -70 and 10 degrees magnetic latitude, and between 7 and 16 hours of local time. Like at Earth, the Parker Spiral angle of the IMF suggests a basic configuration of Mercury's foreshock which should generally cause a correlation between local time and event type, such that – if it were a significant effect – FABs would be more likely to be observed on the dusk side of the planet than the dawn side. Instead, perhaps because of the smaller IMF spiral angle at Mercury and its smaller, more dynamic system, we do not observe a statistically significant asymmetry in the local time of either FAB or diffuse populations in our survey.

As introduced earlier, the population type boundary within the Earth's foreshock is predominantly dependent on θ_{bn} , the angle between the magnetic field and the normal vector to

the shock surface. Therefore, it would be greatly beneficial to discern the origination location of the foreshock events we observed and the conditions there, as well as the local environment these populations occupy. Tracing these events back to the shock surface relies on the analytic bow shock model described in Winslow et al (2013). We used the eccentricity and offset parameters directly from that work, but we tuned the focal parameter to coincide with focal parameter implied by the closest bow shock crossing to the event. For each 10-second accumulation of the FIPS instrument during each FAB and diffuse event period, we traced back from the spacecraft to the bow shock surface in the direction of the average measured magnetic field vector over that period at the spacecraft. This method allows us to recover the local value of θ_{bn} , describing the environment the population occupied at the time of observation. As discussed earlier, we treat the diffuse events as having a very low bulk flow speed in the spacecraft frame. Because the flow speed of the population is very small, possibly even on the order of 10s of km/s, limitations of the spacecraft field of view and noise at low energy prohibit straightforward recovery of its value. Fortunately, given the small magnitude of the bulk flow speed, the local θ_{bn} should be a reasonable estimate of the environment at the origination point for diffuse events.

For FAB events however, which do have a significant bulk velocity in the spacecraft frame, we first calculated the bulk flow direction for the entire event period; then, for each FIPS accumulation, we traced back toward the bow shock surface from the spacecraft's position during that scan along that direction. A rough sketch of the tracing from the spacecraft to the bow shock surface is shown in Figure 8.

The large scatter in upstream locations at which both FAB and diffuse events can be observed speaks to the temporal and spatial variability of the IMF, the solar wind, and the bow shock at Mercury. However, we still expect the populations to be roughly organized by the relevant shock type at their origin, i.e. whether they have their source at a quasi-perpendicular or quasi-parallel bow shock. To this end, after tracing to the bow shock from each FIPS scan, we computed the normal vector to our analytic shock model and compared it with the IMF direction. The IMF at the bow shock is assumed to be the same as that observed by the spacecraft during the scan for which the tracing is performed. The angle between our calculated normal and the measured IMF vector defines θ_{bn} , which in turn determines the drift trajectory of ions at the shock (Gosling et al., 1982).

In the left panel of Figure 9, the calculated local θ_{bn} angle for each scan of each of our foreshock events is histogrammed in bins of 5 degrees. It is evident from inspection of the gold histogram that we preferentially observe diffuse events in the range $\theta_{bn} < 45^\circ$, with a small fraction observed up to 60°. This range is precisely the same as the range observed at Earth in the pioneering work of Bonifazi & Moreno (1981b), who traced diffuse populations back to the shock surface using this same method. However, the diffuse events in our survey differ significantly over that range from results at Earth. Whereas at Earth diffuse populations are seen to peak when the observing spacecraft is connected to a shock with $\theta_{bn}=10^\circ$, we find a somewhat higher peak at around 25°, and a notable lack of observations of diffuse events upstream of the very nearly-parallel shock. The limitations of a single spacecraft require the assumptions of a constant IMF between the spacecraft and the bow shock, and a constant bow shock, which will naturally cause some uncertainty in our estimates of θ_{bn} ; but we do not expect this to be on the order of the difference between these two distributions. That said, other explanations not rooted in unique physics are still possible – after all, the preferential observation of diffuse events in the quasi-parallel shock region at Mercury is still highly consistent with all of

the leading theories behind diffusive shock acceleration at Earth. Examination of the blue histogram in this panel reveals that FABs are observed over approximately the same range as diffuse ions, with a slightly higher average local θ_{bn} . No statistical assessment of the local θ_{bn} of the environment in which FABs are observed at Earth has been performed, but these findings do compare favorably to the modeling results of Jarvinen et al. (2020), who showed a beam population upstream of the quasi-parallel foreshock, and to the expectation from Earth that FABs propagate from the quasi-perpendicular to the quasi-parallel region, where they contribute to the generation of a lively wave environment there.

From examination of the right panel of Figure 9, it is clear to see that our FAB events are observed in the range $10^{\circ} < \theta_{bn} < 75^{\circ}$, with observations tapering off significantly below 25° and above 65°. These results compare extremely favorably with findings at Earth of the origination location for FABs; using the same tracing method, Bonifazi & Moreno (1981b) found that FABs are observed at Earth as having originated from locations on the bow shock with θ_{bn} between 0° and 75°, tapering off significantly below 20° and above 70°. The standard deviation in the local θ_{bn} and estimated θ_{bn} at origination is below 10° for over 92% of cases, with the remainder having standard deviations below 15°.

3.2 Association with Magnetic Field Waves

An important distinction between FAB and diffuse populations observed in Earth's foreshock is the wave signatures associated with each. In the Earth's foreshock there is generally no association between waves (other than from the background wave activity of the foreshock) and the FABs close to the upstream ion foreshock boundary. However, as the FAB distributions widen and scatter in pitch angle, there have been observations of waves in the magnetic field with a frequency close to 1 Hz (spacecraft frame). As one continues deeper into the terrestrial foreshock toward the diffuse population regime of the quasi-parallel shock, the presence of .03 Hz (or 30-sec) waves is seen (Hoppe et al., 1981).

For each of the FAB and diffuse populations in our survey, we have conducted an analysis of the Fourier transform of the magnetic field, in order to investigate the presence of power in any of the three wave modes previously reported in Mercury's foreshock (Le et al., 2013). Table 1 summarizes the distribution of simultaneous wave and plasma observations.

| Wave Mode | Diffuse | FAB |
|-------------------|------------|------------|
| 30-second (.3 Hz) | 87.5% (21) | 6.6% (1) |
| .8 Hz | 8.3% (2) | 73.3% (11) |
| >1 Hz present | 91.7% (22) | 73.3% (11) |

Table 1: Table showing number of observations of FAB and diffuse population survey events associated with simultaneous observation of wave signatures of a particular mode.

Two results are immediately apparent upon inspection of Table 1. Firstly, it is clear to see that the vast majority of events in this survey are associated with waves in the magnetic field of some sort, and that the vast majority of both types of events are associated with the wave mode

>1 Hz. Secondly, we find a clear association between each of the lower-frequency wave modes previously observed at Mercury and the two dominant foreshock plasma populations we have presented. Like at Earth, we find that diffuse populations are associated with the "30-second" waves, with a frequency at Mercury of roughly 0.3 Hz. Unlike at Earth, we find that FABs are also associated with a wave mode – the previously observed, but as-yet unexplained, 0.8 Hz waves. Although analysis of the magnetic field in greater detail is beyond the scope of this survey of plasma measurements, we are encouraged by the possibilities for future study into the origin of this 0.8 Hz wave mode at Mercury, now that its association with a plasma phenomenon is known. Note, however, that association with a particular plasma phenomenon does not necessarily imply a causal link between the two; the 30-second mode is itself an excellent example of why caution is warranted, given its simultaneous observation at Earth and now at Mercury with diffuse populations, despite being best explained at Earth as generated by FABs.

Figure 10 shows the ratio between the FAB velocity in the solar wind frame and the solar wind speed. Although our event count is fewer than we might like for well-refined statistics, this distribution compares quite favorably to Figure 4a of Romanelli et al. (2020), which provides a summary of the predicted ratio between the interacting particles in the solar wind frame and the solar wind speed, based on statistical observations of the 30-second waves at Mercury. The anticipated speed ratio of resonant particles to the solar wind ranges in that study between .9 and 2.6, with a mean between 1.7 and 1.8; we find that the actual speed ratio for FABs in our study ranges between .95 and 2.77, with a mean value of about 2.05. One potential explanation for the slight difference between these results is that because resonant particles are already interacting with waves, we expect they have lost some energy, and therefore that the ratio computed through wave activity will be slightly smaller than the ratio observed before wave interaction commences; however, the former quantity is difficult to ascertain from our plasma measurements, so the extent of the difference this would cause is not easy to capture. Nonetheless, the similarity in these results despite the very different approach compels the conclusion that, just as in the terrestrial foreshock, FABs at Mercury are connected to the generation of waves in the diffuse foreshock region, notwithstanding the vast differences in sizes of the two shocks and parameter regimes at the two planets (see Romanelli & DiBraccio, 2021 for further discussion of the effect of the dynamic upstream environment on Mercury's 30-second waves).

Conclusions

This is the first comprehensive application of the plasma measurements of the FIPS instrument to understanding Mercury's foreshock environment. The FAB and diffuse plasma populations are successfully identified and quantified using the full directional capabilities of the FIPS instrument. Overall, the findings of this survey tell a story of a foreshock that is broadly very similar to the terrestrial foreshock, but with some minor – but compelling – differences. For example, the organization of the foreshock populations by θ_{bn} is confirmed at Mercury to be substantially similar to the organization of the foreshock at Earth, with FAB populations preferentially observed over a range from $\theta_{bn} = [30^o, 70^o]$ and with a mean value extremely consistent with that at Earth. Also like Earth, the diffuse populations in our survey are observed over $\theta_{bn} = [10^o, 40^o]$. However, the observations of diffuse plasma in this survey peak when the spacecraft is connected to a shock with $\theta_{bn} = 25^\circ$, contrasting to the peak of 10° at Earth. A survey of significantly more diffuse events at Mercury would be required to confirm the statistical significance of this finding.

Separately, we have shown that a correlation exists between magnetic wave activity modes (previously observed at Earth to be connected to foreshock plasma) and the observed plasma populations in Mercury' foreshock. As far as magnetic field waves are concerned, it is the diffuse populations which show complete consistency with Earth observations; we find that these populations are associated with simultaneous observation of the so-called "30-second waves" and >1Hz whistler mode waves, both of which are observed at Earth to be associated with diffuse populations. In contrast, although the FABs we observe are highly consistent with the anticipated generation mechanism for these 30-second waves, the FABs in our survey are also concurrently associated with the 0.8 Hz wave mode previously observed to be unique to Mercury. This stands in contrast to Earth, where FABs are not observed simultaneously with any unique wave mode. Both of these differences to the terrestrial system are worthy of further investigation in a larger statistical survey.

Measurements of the foreshock plasma populations at Mercury provide constraints for current theories of particle acceleration in the foreshock. We encourage future work on how the features of the diffuse plasma observed at Mercury can inform the current understanding of diffusive shock acceleration at Earth. For example, the small spatial scale of Mercury's bow shock may be the ideal environment to investigate finite connection time limited acceleration. Quantifying the spatial profile of the diffuse foreshock plasma will also inform theories of diffusive shock acceleration. In addition, application of the method of (Paschmann et al., 1980) already known to work at Earth's foreshock for predicting FAB energization can now be applied more broadly to test if it is similarly applicable, despite the vastly different ambient conditions, at Mercury.

Confirmation that FABs and diffuse populations are generated in Mercury's foreshock also opens up opportunities for future analysis of other features common to the remaining three terrestrial planetary shocks, at Venus, Earth, and Mars. These include foreshock cavities, which have been observed at all three planets (Collinson et al., 2020). Modeling has demonstrated that these cavities can transform into Spontaneous Hot Flow Anomalies (SHFAs) at Alfvénic Mach numbers greater than about 3 (Omidi et al., 2014). Given that the Alfvénic Mach number of the solar wind at Mercury's orbital distance from the Sun can occasionally fall below 3 (Sarantos & Slavin, 2009), Mercury may represent a unique planetary environment for the investigation of the particular conditions necessary for SHFA generation, which are certainly present in the other three terrestrial foreshocks (Collinson et al., 2017). Our results also encourage investigation of the foreshock compression boundary at Mercury, which bounds the region of high ULF wave activity in other terrestrial foreshocks (Omidi et al., 2009). In fact, at least one event included in our survey may even present an opportunity for observation of foreshock cavities and compression boundaries – see respectively the overall depression (and significant shorter depressions) of magnetic field strength from 06:41 to 06:49 UTC in Figure 5, preceded by the small bump in magnetic field strength at around 06:38:30 UTC. Note, however, that significant further analysis will be necessary to draw any concrete conclusions about the presence of such features at Mercury.

Finally, the measurements reported in this work set an important precedent for comparison with future measurements of Mercury's foreshock. The BepiColombo mission will arrive at Mercury in 2025 and consist of two spacecraft: the Mercury Planetary Orbiter (MPO) and the Mercury Magnetospheric Orbiter (MMO). On the MMO spacecraft, the instruments of the Mercury Plasma Particle Experiment (MPPE) including the Mercury Ion Anlyzer (MIA),

Mercury Spectrum Analyzer (MSA), and High-Energy Particle instrument for ions (HEP-ion) will collectively sample ions at energies from 5 eV to 1500 keV (Saito et al., 2010). The broader range of energies measured by these instruments will enable further investigation and understanding of shock acceleration mechanisms in the unique Hermean foreshock parameter regime.

Acknowledgments

Portions of this work are derived from the doctoral dissertation of PJT. The MESSENGER project has been supported by the NASA Discovery Program under contracts NAS5-97271 to The Johns Hopkins University Applied Physics Laboratory and NASW-00002 to the Carnegie Institution of Washington. MESSENGER FIPS and MAG data are available through the NASA Planetary Data System. NASA's Astrophysics Data System was used extensively for this work. Some of the work performed by ANG was also funded under the Undergraduate Research Opportunities Program at the University of Michigan. NR is supported through a cooperative agreement with Center for Research and Exploration in Space Sciences & Technology II (CRESST II) between NASA Goddard Space Flight Center and University of Maryland College Park under award No. 80GSFC21M0002. We also acknowledge the contributions of an anonymous reviewer on the potential broader implications of the observations displayed in Figure 5, presented in Conclusions.

Open Research

FIPS data are publicly available for download through the NASA Planetary Data System, including through the MESSENGER EPPS respository at https://doi.org/10.17189/1519742. MAG data are also available through NASA PDS, at https://doi.org/10.17189/1522383.

References

- Anderson, B. J., Acuña, M. H., Lohr, D. A., Scheifele, J., Raval, A., Korth, H., & Slavin, J. A. (2007). The magnetometer instrument on MESSENGER. *Space Science Reviews*, *131*(1–4), 417–450. https://doi.org/10.1007/s11214-007-9246-7
- Andrews, G. B., Zurbuchen, T. H., Mauk, B. H., Malcom, H., Fisk, L. A., Gloeckler, G., et al. (2007). The energetic particle and plasma spectrometer instrument on the MESSENGER spacecraft. *Space Science Reviews*, *131*(1–4), 523–556. https://doi.org/10.1007/s11214-007-9272-5
- Blanco-Cano, X., Omidi, N., & Russell, C. T. (2006). Macrostructure of collisionless bow shocks: 2. ULF waves in the foreshock and magnetosheath. *Journal of Geophysical Research: Space Physics*, *111*(10). https://doi.org/10.1029/2005JA011421
- Bonifazi, C., & Moreno, G. (1981a). Reflected and diffuse ions backstreaming from the Earth's bow shock 1. Basic properties. *Journal of Geophysical Research: Space Physics*, 86(A6), 4397–4404. https://doi.org/10.1029/ja086ia06p04397
- Bonifazi, C., & Moreno, G. (1981b). Reflected and diffuse ions backstreaming from the Earth's bow shock 2. Origin. *Journal of Geophysical Research: Space Physics*, 86(A6), 4405–4413. https://doi.org/10.1029/ja086ia06p04405
- Burgess, D. (1989). Alpha particles in field-aligned beams upstream of the bow shock: Simulations. *Geophysical Research Letters*, *16*(2), 163–166. https://doi.org/10.1029/GL016i002p00163

- Burgess, D., Möbius, E., & Scholer, M. (2012). Ion acceleration at the earth's bow shock. *Space Science Reviews*, 173(1–4), 5–47. https://doi.org/10.1007/s11214-012-9901-5
- Burgess, David. (1987). Shock drift acceleration at low energies. *Journal of Geophysical Research*, 92(A2), 1119. https://doi.org/10.1029/ja092ia02p01119
- Collinson, G., Sibeck, D., Omidi, N., Grebowsky, J., Halekas, J., Mitchell, D., et al. (2017). Spontaneous hot flow anomalies at Mars and Venus. *Journal of Geophysical Research: Space Physics*, *122*(10), 9910–9923. https://doi.org/10.1002/2017JA024196
- Collinson, G., Sibeck, D., Omidi, N., Frahm, R., Zhang, T., Mitchell, D., et al. (2020). Foreshock Cavities at Venus and Mars. *Journal of Geophysical Research: Space Physics*, *125*(8), e2020JA028023. https://doi.org/10.1029/2020JA028023
- Edmiston, J. P., Kennel, C. F., & Eichler, D. (1982). Escape of heated ions upstream of quasiparallel shocks. *Geophysical Research Letters*, 9(5), 531–534. https://doi.org/10.1029/GL009i005p00531
- Fairfield, D. H., & Behannon, K. W. (1976). Bow Shock and Magnetosheath Waves At Mercury. *J Geophys Res*, 81(22), 3897–3906. https://doi.org/10.1029/JA081i022p03897
- Gary, S. P., Gosling, J. T., & Forslund, D. W. (1981). The electromagnetic ion beam instability upstream of the Earth's bow shock. *Journal of Geophysical Research*, *86*(A8), 6691. https://doi.org/10.1029/ja086ia08p06691
- Gershman, D. J., Zurbuchen, T. H., Fisk, L. A., Gilbert, J. A., Raines, J. M., Anderson, B. J., et al. (2012). Solar wind alpha particles and heavy ions in the inner heliosphere observed with MESSENGER. *Journal of Geophysical Research: Space Physics*, *117*(9). https://doi.org/10.1029/2012JA017829
- Gershman, D. J., Slavin, J. A., Raines, J. M., Zurbuchen, T. H., Anderson, B. J., Korth, H., et al. (2013). Magnetic flux pileup and plasma depletion in Mercury's subsolar magnetosheath. *Journal of Geophysical Research: Space Physics*, *118*(11), 7181–7199. https://doi.org/10.1002/2013JA019244
- Gosling, J. T., Thomsen, M. F., Bame, S. J., Feldman, W. C., Paschmann, G., & Sckopke, N. (1982). Evidence for specularly reflected ions upstream from the quasi-parallel bow shock. *Geophysical Research Letters*, *9*(12), 1333–1336. https://doi.org/10.1029/GL009i012p01333
- Gosling, J. T., Thomsen, M. F., Bame, S. J., & Russell, C. T. (1989). On the source of diffuse, suprathermal ions observed in the vicinity of the Earth's bow shock. *Journal of Geophysical Research*, 94(A4), 3555. https://doi.org/10.1029/ja094ia04p03555
- Hoppe, M. M., Russell, C. T., Frank, L. A., Eastman, T. E., & Greenstadt, E. W. (1981). Upstream hydromagnetic waves and their association with backstreaming ion populations: ISEE 1 and 2 observations. *Journal of Geophysical Research: Space Physics*, 86(A6), 4471–4492. https://doi.org/10.1029/ja086ia06p04471
- Ipavich, F. M., Gloeckler, G., Fan, C. Y., Fisk, L. A., Hovestadt, D., Klecker, B., et al. (1979). Initial observations of low energy charged particles near the Earth's bow shock on ISEE-1. *Space Science Reviews*, 23(1), 93–101. https://doi.org/10.1007/BF00174113

Ipavich, F. M., Gosling, J. T., & Scholer, M. (1984). CORRELATION BETWEEN THE He/H

RATIOS IN UPSTREAM PARTICLE EVENTS AND IN THE SOLAR WIND. *Journal of Geophysical Research*, 89(A3), 1501–1507. https://doi.org/10.1029/JA089iA03p01501

- Ipavich, F. M., Gloeckler, G., Hamilton, D. C., Kistler, L. M., & Gosling, J. T. (1988). Protons and alpha particles in field-aligned beams upstream of the bow shock. *Geophysical Research Letters*, *15*(10), 1153–1156. https://doi.org/10.1029/GL015i010p01153
- Jarvinen, R., Alho, M., Kallio, E., & Pulkkinen, T. I. (2020). Ultra-low-frequency waves in the ion foreshock of Mercury: A global hybrid modelling study. *Monthly Notices of the Royal Astronomical Society*, 491(3), 4147–4161. https://doi.org/10.1093/mnras/stz3257
- Kempf, Y., Pokhotelov, D., Gutynska, O., Wilson, L. B., Walsh, B. M., Alfthan, S. Von, et al. (2015). Ion distributions in the Earth's foreshock: Hybrid-Vlasov simulation and THEMIS observations. *Journal of Geophysical Research: Space Physics*, *120*(5), 3684–3701. https://doi.org/10.1002/2014JA020519
- Kis, A., Scholer, M., Klecker, B., Möbius, E., Lucek, E. A., Rème, H., et al. (2004). Multispacecraft observations of diffuse ions upstream of earth's bow shock. *Geophysical Research Letters*, *31*(20). https://doi.org/10.1029/2004GL020759
- Kis, A., Scholer, M., Klecker, B., Kucharek, H., Lucek, E. A., & Rème, H. (2007). Scattering of field-aligned beam ions upstream of Earth's bow shock. *Annales Geophysicae*, *25*(3), 785–799. https://doi.org/10.5194/angeo-25-785-2007
- Kucharek, H., Möbius, E., Scholer, M., Mouikis, C., Kistler, L. M., Horbury, T., et al. (2004). On the origin of field-aligned beams at the quasi-perpendicular bow shock: Multi-spacecraft observations by Cluster. *Annales Geophysicae*, 22(7), 2301–2308. https://doi.org/10.5194/angeo-22-2301-2004
- Le, G., Chi, P. J., Blanco-Cano, X., Boardsen, S., Slavin, J. A., Anderson, B. J., & Korth, H. (2013). Upstream ultra-low frequency waves in Mercury's foreshock region: MESSENGER magnetic field observations. *Journal of Geophysical Research: Space Physics*, *118*(6), 2809–2823. https://doi.org/10.1002/jgra.50342
- Möbius, E., Kucharek, H., Mouikis, C., Georgescu, E., Kistler, L. M., Popecki, M. A., et al. (2001). Observations of the spatial and temporal structure of field-aligned beam and gyrating ring distributions at the quasi-perpendicular bow shock with Cluster CIS. *Annales Geophysicae*, *19*(10/12), 1411–1420. https://doi.org/10.5194/angeo-19-1411-2001
- Ogilvie, K. W., Scudder, J. D., Vasyliunas, V. M., Hartle, R. E., & Siscoe, G. L. (1977). Observations at the planet Mercury by the Plasma Electron Experiment: Mariner 10. *Journal of Geophysical Research*, 82(13), 1807–1824. https://doi.org/10.1029/ja082i013p01807
- Oka, M., Terasawa, T., Saito, Y., & Mukai, T. (2005). Field-aligned beam observations at the quasi-perpendicular bow shock: Generation and shock angle dependence. *Journal of Geophysical Research: Space Physics*, *110*(A5). https://doi.org/10.1029/2004JA010688
- Omidi, N., Blanco-Cano, X., & Russell, C. T. (2005). Macrostructure of collisionless bow shocks: 1. Scale lengths. *Journal of Geophysical Research: Space Physics*, *110*(A12). https://doi.org/10.1029/2005JA011169
- Omidi, N., Sibeck, D. G., & Blanco-Cano, X. (2009). Foreshock compressional boundary.

Journal of Geophysical Research: Space Physics, 114(A8), n/a-n/a. https://doi.org/10.1029/2008ja013950

- Omidi, N., Sibeck, D., Gutynska, O., & Trattner, K. J. (2014). Magnetosheath filamentary structures formed by ion acceleration at the quasi-parallel bow shock. *Journal of Geophysical Research: Space Physics*, *119*(4), 2593–2604. https://doi.org/10.1002/2013JA019587
- Parks, G. K., Lee, E., Fu, S. Y., Lin, N., Liu, Y., & Yang, Z. W. (2017). Shocks in collisionless plasmas. *Reviews of Modern Plasma Physics*, 1(1), 1. https://doi.org/10.1007/s41614-017-0003-4
- Paschmann, G., Sckopke, N., Bame, S. J., Asbridge, J. R., Gosling, J. T., Russell, C. T., & Greenstadt, E. W. (1979). Association of low-frequency waves with suprathermal ions in the upstream solar wind. *Geophysical Research Letters*, 6(3), 209–212. https://doi.org/10.1029/GL006i003p00209
- Paschmann, G., Sckopke, N., Asbridge, J. R., Bame, S. J., & Gosling, J. T. (1980). Energization of solar wind ions by reflection from the Earth's bow shock. *Journal of Geophysical Research: Space Physics*, 85(A9), 4689–4693. https://doi.org/10.1029/ja085ia09p04689
- Paschmann, G., Sckopke, N., Papamastorakis, I., Asbridge, J. R., Bame, S. J., & Gosling, J. T. (1981). Characteristics of reflected and diffuse ions upstream from the Earth's bow shock. *Journal of Geophysical Research: Space Physics*, 86(A6), 4355–4364. https://doi.org/10.1029/ja086ia06p04355
- Romanelli, N., & DiBraccio, G. A. (2021). Occurrence rate of ultra-low frequency waves in the foreshock of Mercury increases with heliocentric distance. *Nature Communications*, 12(1), 6748. https://doi.org/10.1038/s41467-021-26344-2
- Romanelli, N., DiBraccio, G., Gershman, D., Le, G., Mazelle, C., Meziane, K., et al. (2020). Upstream Ultra-Low Frequency Waves Observed by MESSENGER's Magnetometer: Implications for Particle Acceleration at Mercury's Bow Shock. *Geophysical Research Letters*, 47(9), e2020GL087350. https://doi.org/10.1029/2020GL087350
- Saito, Y., Sauvaud, J. A., Hirahara, M., Barabash, S., Delcourt, D., Takashima, T., & Asamura, K. (2010). Scientific objectives and instrumentation of Mercury Plasma Particle Experiment (MPPE) onboard MMO. *Planetary and Space Science*, *58*(1), 182–200. https://doi.org/https://doi.org/10.1016/j.pss.2008.06.003
- Sarantos, M., & Slavin, J. A. (2009). On the possible formation of Alfvén wings at Mercury during encounters with coronal mass ejections. *Geophysical Research Letters*, *36*(4). https://doi.org/10.1029/2008GL036747
- Shan, L., Mazelle, C., Meziane, K., Delva, M., Lu, Q., Ge, Y. S., et al. (2016). Characteristics of quasi-monochromatic ULF waves in the Venusian foreshock. *Journal of Geophysical Research: Space Physics*, *121*(8), 7385–7397. https://doi.org/10.1002/2016JA022876
- Shan, L., Mazelle, C., Meziane, K., Romanelli, N., Ge, Y. S., Du, A., et al. (2018). The Quasimonochromatic ULF Wave Boundary in the Venusian Foreshock: Venus Express Observations. *Journal of Geophysical Research: Space Physics*, *123*(1), 374–384. https://doi.org/10.1002/2017JA024054

Slavin, J. A., & Holzer, R. E. (1981). Solar wind flow about the terrestrial planets 1. Modeling bow shock position and shape. *Journal of Geophysical Research*, 86(A13), 11401. https://doi.org/10.1029/ja086ia13p11401

Sonnerup, B. U. Ö. (1969). Acceleration of particles reflected at a shock front. *Journal of Geophysical Research*, 74(5), 1301–1304. https://doi.org/10.1029/ja074i005p01301

Tanaka, M., Goodrich, C. C., Winske, D., & Papadopoulos, K. (1983). A source of the backstreaming ion beams in the foreshock region. *Journal of Geophysical Research*, 88(A4), 3046. https://doi.org/10.1029/ja088ia04p03046

Winske, D., & Leroy, M. M. (1984). Diffuse Ions Produced By Electromagnetic Ion Beam Instabilities. *Journal of Geophysical Research*, 89(A5), 2673–2688.
https://doi.org/10.1029/JA089iA05p02673

 Winslow, R. M., Anderson, B. J., Johnson, C. L., Slavin, J. A., Korth, H., Purucker, M. E., et al. (2013). Mercury's magnetopause and bow shock from MESSENGER Magnetometer observations. *Journal of Geophysical Research: Space Physics*, *118*(5), 2213–2227. https://doi.org/10.1002/jgra.50237

Yamauchi, M., Futaana, Y., Fedorov, A., Frahm, R. A., Winningham, J. D., Dubinin, E., et al. (2011). Comparison of accelerated ion populations observed upstream of the bow shocks at Venus and Mars. *Annales Geophysicae*, *29*(3), 511–528. https://doi.org/10.5194/angeo-29-511-2011

Zhang, H., Zong, Q., Connor, H., Delamere, P., Facskó, G., Han, D., et al. (2022). Dayside Transient Phenomena and Their Impact on the Magnetosphere and Ionosphere. *Space Science Reviews*, 218(5), 40. https://doi.org/10.1007/s11214-021-00865-0

Figure 1: Energy spectrogram (top panel), Pitch Angle distribution (second panel), MSO X, Y, and Z components of the magnetic field and magnetic field magnitude (remaining panels), all as a time series of data measured over a single orbit of the MESSENGER spacecraft. The higher energy particles roughly between 14:20 and 15:00 (red lines) are the observed FAB plasma population.

Figure 2: All-sky map of the ions between .3 and 1 keV during the foreshock population event period of Figure 1. A portion of the solar wind beam can be seen around the white shaded portion of the FIPS FoV, because of its thermal width and because it is aberrated in the spacecraft frame in the dusk direction due to planetary motion. Also shown on the figure is the average vector magnetic field direction; the magenta circle with a dot is the +B direction, while the magenta circle with the X is the -B direction.

Figure 3: Energy-resolved pitch angle distributions over the FAB period, Sept 19th, 2012, 14:25-15:00. The left distribution, ranging from 0.3-1 keV, shows the solar wind in the spacecraft frame. The right distribution shows a purely backstreaming field-aligned beam in the solar wind frame at energies above 1 keV.

Figure 4: Top panel: Measured count distribution of protons. Green points indicate the lower energy solar wind portion, and blue points the higher energy FAB population. Bottom panel: the calculated phase space density distribution, with the same color scheme. The dashed line represents the "one-count" line in phase space. The recovered plasma parameters for the solar wind and FAB population are shown in the plot title. Adapted from Tracy (2016).

Figure 5: Top panel: time series energy spectrogram from 6:30 to 7:40 UTC on Dec. 5, 2012, showing a short period of observation of a diffuse population followed by a longer period starting at 6:40, which ends at the bow shock crossing at around 7:22. Remaining panels: popped out zoom of a portion of the diffuse event period in the foreshock, in the style of Figure 1.

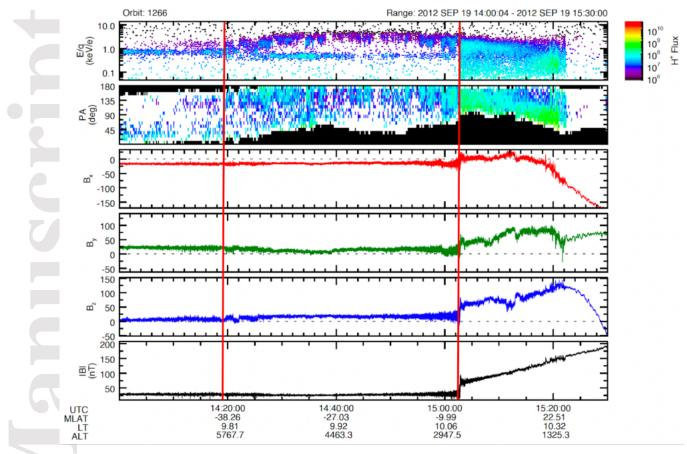
Figure 6: An energy-resolved pitch angle distribution over the diffuse event period, Dec 5th, 2012, 6:30-7:00, in the solar wind reference frame. The distribution is wide in angle and hot, spanning well over an order of magnitude in energy.

Figure 7: Count and phase space density distribution during the diffuse observation event period, in the style of Figure 4. The recovered plasma parameters for the solar wind and diffuse population are shown in the plot title.

Figure 8: Sketch of the tracing scheme for populations in the Hermean foreshock. Traces along both the IMF direction and the FAB propagation direction relative to the spacecraft (shown as a star) are indicated. The light green line represents the trace along the IMF direction toward the shock, and is applied to both FABs and diffuse events. The dark blue line represents the trace back along the FAB vector direction. At the point these traces intersect the bow shock surface, normals to the surface are depicted.

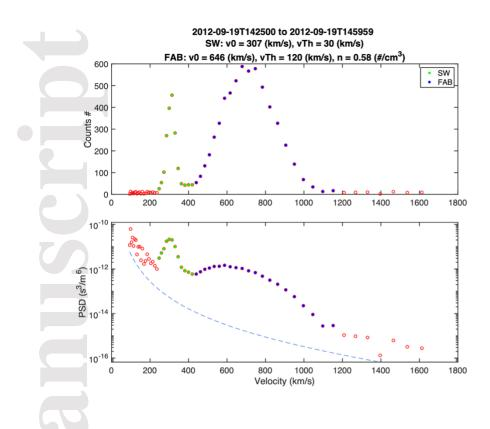
Figure 9: Two histograms of the relative frequency of the recovered angle between the bow shock normal and the IMF B field. At left, the local value of this angle is shown, and at the right, the estimated value at the FAB origination point is shown.

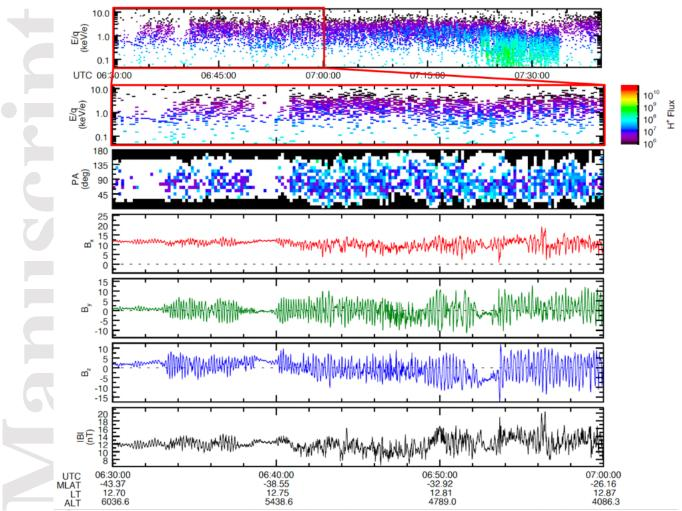
Figure 10: The ratio between FAB speed in the solar wind frame and and the solar wind speed in the spacecraft frame for the events in our survey. Despite low statistics, the distribution shows good agreement in mean and range with a similar figure from Romanelli et al. (2020).



A uthor N







Author

